A sumatriptan coarse-grained model to explore different environments: interplay with experimental techniques

9 authors, including:

Irene Wood
Universidad de la República de Uruguay
8 PUBLICATIONS **52** CITATIONS

SEE PROFILE

Marcelo Alexandre De Farias
Centro Nacional de Pesquisa em Energia e Materiais
26 PUBLICATIONS **106** CITATIONS

SEE PROFILE

Rodrigo Villares Portugal
Centro Nacional de Pesquisa em Energia e Materiais
49 PUBLICATIONS **228** CITATIONS

SEE PROFILE

Eneida de Paula
University of Campinas
256 PUBLICATIONS **3,345** CITATIONS

SEE PROFILE

Some of the authors of this publication are also working on these related projects:

Project Carbon nanotube hybrid polymer composites View project
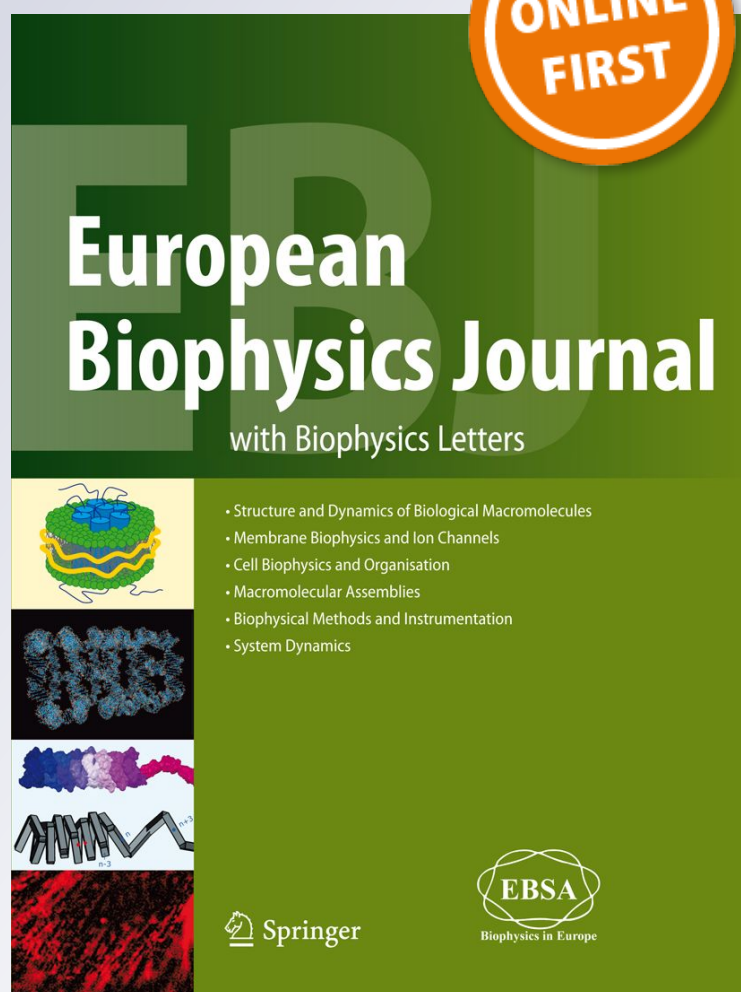
Project targeted nano-inmmunomodulator View project

A sumatriptan coarse-grained model to explore different environments: interplay with experimental techniques

Irene Wood, Juan M. R. Albano, Pedro L. O. Filho, Veronica Muniz Couto, Marcelo A. de Farias, Rodrigo V. Portugal, Eneida de Paula, et al.

European Biophysics Journal
with Biophysics Letters

- Structure and Dynamics of Biological Macromolecules
- Membrane Biophysics and Ion Channels
- Cell Biophysics and Organisation
- Macromolecular Assemblies
- Biophysical Methods and Instrumentation
- System Dynamics

Springer

EBSA
Biophysics in Europe

Springer

Springer

ORIGINAL ARTICLE

A sumatriptan coarse-grained model to explore different environments: interplay with experimental techniques

Irene Wood[1,2] · Juan M. R. Albano[1,2] · Pedro L. O. Filho[4] · Veronica Muniz Couto[3] · Marcelo A. de Farias[5] ·
Rodrigo V. Portugal[5] · Eneida de Paula[3] · Cristiano L. P. Oliveira[4] · Monica Pickholz[1,2]

Abstract
In this work, we developed a coarse-grained model of sumatriptan suitable for extensive molecular dynamics simulations. First, we confirmed the interfacial distribution of this drug in bilayers through cryogenic transmission electron microscopy and small-angle X-ray scattering techniques, as was predicted by our previous atomistic simulations. Based on these simulations, we developed a coarse-grained model for sumatriptan able to reproduce its overall molecular behavior, captured by atomistic simulations and experiments. We then tested the sumatriptan model in a micellar environment along with experimental characterization of sumatriptan-loaded micelles. The simulation results showed good agreement with photon correlation spectroscopy and electrophoretic mobility experiments performed in this work. The particle size of the obtained micelles was comparable with the simulated ones; meanwhile, zeta-potential results suggest adsorption of the drug on the micellar surface. This model is a step forward in the search for a suitable drug-delivery system for sumatriptan.

Keywords Molecular dynamics · Sumatriptan · Coarse-grained model · SAXS · Cryo-TEM

Irene Wood and Juan M. R. Albano contributed equally to this work.

Electronic supplementary material The online version of this article (https://doi.org/10.1007/s00249-018-1278-2) contains supplementary material, which is available to authorized users.

✉ Monica Pickholz
monicapickholz@gmail.com

1 Departamento de Física, Facultad de Ciencias Exactas y Naturales, Universidad de Buenos Aires, Buenos Aires, Argentina

2 Instituto de Física de Buenos Aires (IFIBA), CONICET–Universidad de Buenos Aires, Buenos Aires, Argentina

3 Instituto de Biologia, University of Campinas, Campinas, SP 13083-862, Brazil

4 Institute of Physics, University of São Paulo, Rua do Matão, 1371, São Paulo, SP CEP 05508-090, Brazil

5 Brazilian Nanotechnology National Laboratory (LNNano), Brazilian Center for Research in Energy and Materials (CNPEM), Campinas, SP 13083-970, Brazil

Introduction

Triptans are a drug family designed for the treatment of acute migraine. All triptans share an indole structure with the neurotransmitter serotonin and most of them contain side chains, with a basic nitrogen and a sulfonamide group (Tepper et al. 2002). Sumatriptan (SMT) was the first and most used member of this family. The hydrophilicity of this drug, evidenced through its low partition coefficient in n-octanol/water ($\log P = 1.2$), hinders its access to the central nervous system (CNS) (Tfelt-Hansen 2010). The development of drug-delivery systems for hydrophilic drugs such as SMT is currently the most promising strategy aiming to minimize side effects, to sustain drug release/effect, and also to facilitate its permeation across the blood–brain barrier, targeting the brain. Recently, some attempts to encapsulate SMT in nanoparticles were made (Gulati 2013; Hansraj et al. 2015; Girotra and Singh 2016). However, just a few of them have resulted in viable pharmaceutical solutions; therefore, new strategies are still necessary to improve them. In this direction, the rational development of nanocarriers would be extremely useful, especially using computational methods (Haddish-Berhane et al. 2007).

In order to get insight on nanoparticle structure and dynamics, molecular dynamics (MD) simulations represent a powerful tool (Karplus and McCammon 2002). Fully atomistic (AA) treatment of these kinds of systems could bring interesting information on its properties but, in this scheme, the systems must be represented partially or with over-simplification. Therefore, an attractive solution is to treat the whole system at a coarse-grain (CG) level, reducing the degrees of freedom by grouping atoms at specific sites (Horn and Kao 2014). In this direction, the systematic use of MD could help in the search for suitable drug-delivery systems for a specific drug (Haddish-Berhane et al. 2007). The first step within this approach is to obtain a CG parameterization for the drugs and macromolecules of interest. To the best of our knowledge, no SMT CG model has been reported in the literature.

In a previous work, using atomistic MD simulations, we addressed the SMT interaction with model membranes comparing different conditions (Wood and Pickholz 2013, 2014). The main results pointed out the interfacial distribution of SMT. Furthermore, the AA simulations allow us to identify the specific interactions responsible for this behavior: cation-π, salt bridges, and hydrogen bonds between SMT structure and lipid head groups. A reliable SMT CG model should be able to reproduce the atomistic simulated distributions, as well as SMT experimental behavior.

In this work, we propose a CG model for SMT based on atomistic simulations and experimental data. Experimental techniques, such as cryogenic transmission electron microscopy (Cryo-TEM) and small-angle X-ray scattering (SAXS), are used to study the interaction of SMT with liposomes. To further evaluate our model, we simulate the encapsulation of CG SMT into nanocarriers, such as polymeric micelles, and perform experimental measurements (photon correlation spectroscopy/electrophoretic mobility) to correlate with the simulation predictions.

Materials and methods

Sample preparation

Liposomes

Egg phosphatidylcholine liposomes (EPC) (Avanti Polar Lipids, Alabaster, AL, USA) were prepared at a final lipid concentration of 20 mM. First, lipids were dissolved in chloroform. Then, the solvent was removed under nitrogen flux to form a thin lipid film (Cereda et al. 2006). In order to remove any chloroform residue, the film was left to dry in a vacuum for 2 h. Afterwards, it was hydrated with phosphate buffer (pH 7.4) containing SMT, at different concentrations. This solution was vortexed (3 min) to form the vesicles. The liposome was extruded through a polycarbonate membrane (400 nm) to narrow size distribution (Patil and Jadhav 2014). For SAXS and Cryo-TEM experiments, the samples were prepared at different drug:lipid molar ratios (0:1–1:3–1:2 and 0:1–1:3–11:1, respectively).

Micelles

Pluronic (PL) F127 (MW 12,500 g/mol and CMC = 0.725 wt% at 25 °C) was purchased from Sigma-Aldrich (USA) and used without further purification. Pure F127 suspensions were prepared above its critical micellar concentration (CMC) at 8 wt% by dissolving appropriate amounts of F127 in deionized water under vigorous stirring at cold condition (0–8 °C) for 6 h (Sharma and Bhatia 2004; Zhang and Lam 2007). Then, SMT was actively loaded into the micelles, at 0:1 and 1:1 molar ratio SMT:PL F127, under stirring.

Experimental setup

SAXS

SAXS measurements were performed using a Bruker-NANOSTAR located at the Laboratory of Crystallography at the Institute of Physics of the University of São Paulo. This camera is equipped with a microfocus Genix 3D system (source and focusing mirrors) and two scatterless slit sets for collimation, both provided by Xenocs. The detection was performed by a Vantec-2000 area detector. Scattering experiments on the liquid samples were performed using reusable homemade sample holders composed of quartz capillaries glued on stainless-steel cases. Background intensities were obtained based on scattering by the corresponding buffers measured using the same capillaries. The data were obtained by frames of 1800 s. Data treatment, normalization, and averaging were performed using the package SUPERSAXS (Pedersen et al. 2012).

Cryo-TEM

Cryo-TEM grids were prepared using an automated vitrification system (Vitrobot Mark IV, Thermo Fisher Scientific, Waltham, MA, USA) as discussed before (Gasperini et al. 2015). Specimens were analyzed in low-dose condition with a defocus range of − 2 to − 4 µm using a Jeol JEM-1400 Plus electron microscope operating at 120 kV. Images were acquired using a Gatan Multi-Scan 794 CCD camera.

DLS and Zeta potential

Photon correlation/dynamic light scattering (DLS), performed in a Zeta sizer Nano ZS90 (Malvern, United

Kingdom) was used to determine the polymeric micellar hydrodynamic diameter and size distribution (polydispersity) (Hassan et al. 2015). The samples were diluted in deionized water and measured three times at 37 and 45 °C with a scattering angle of 90°. Using the same equipment, the zeta potential of the particles was determined by electrophoretic mobility (Ito et al. 2004).

Simulation setup

The development of the SMT CG model was based on MARTINI Force Field (MFF) (Marrink et al. 2007). The MARTINI CG model allows a systematic representation of molecules in terms of a few building blocks (CG beads) that can be used in a broad range of biomolecular applications (Monticelli et al. 2008). Within MFF, many kinds of water models and lipid molecules are fully parameterized (Marrink et al. 2007), including the POPC used here. For PL F127, the parameters were taken from our previous work (Wood et al. 2016). In all cases, polarizable water was used (Yesylevskyy et al. 2010). MFF chlorine was added as counter-ion in the same amount as SMT in order to maintain charge neutrality.

All CG MD simulations were performed using GROMACS 4.5 software (Hess et al. 2008). A cut-off of 12 Å was applied for the Lennard–Jones (LJ) and electrostatic interactions. A global dielectric constant of $\varepsilon_r = 2.5$ was set to ensure a realistic dielectric behavior of the hydrophobic regions using the polarizable water model (Yesylevskyy et al. 2010). We have carried out the simulations within an ensemble of a constant number of molecules, pressure, and temperature (NPT) within periodic boundary conditions. The pressure and temperature were kept constant ($P = 1$ bar and $T = 300$ K) using the Berendsen thermostat and barostat (Berendsen et al. 1984) with a coupling constant of 0.3 ps for temperature and pressure, and compressibility of 3×10^5 bar^{-1}. A time step of 10 fs was used.

Results and discussion

Sumatriptan interaction with lipid bilayers: building up the coarse-grained model

Liposomes are lipid vesicles of spherical shape widely used as a versatile tool for biomimetic systems (Steichen et al. 2013). Their composition can vary from naturally derived phospholipids with mixed lipid chains like EPC, to pure lipid components like POPC. Because of the amphipathic nature of these lipid molecules, they spontaneously assemble in water into bilayer structures. In these kinds of bilayers, the lipids' hydrophilic heads interact with the water, forming a complex interface, and their acyl chain tails compose the hydrophobic core. Besides,

liposomes are composed of one or more bilayers that present a characteristic repetitive inter-bilayer spacing, called *D*-spacing. This *D*-spacing represents the bilayer thickness or lamellar size (δm) plus the water between the bilayers, as schematized in Fig. 1. Both *D*-spacing and δm characterize the vesicle, being very sensitive to small perturbations (i.e., the presence of small molecules, temperature, and pH). Cryo-TEM and SAXS are experimental techniques that can yield *D*-spacing and δm properties. The first technique allows estimating the *D*-spacing and δm of selected liposome images while the second has better precision since the results are obtained from an average of a large number of particles. The δm can be correlated with the bilayer thickness obtained by MD simulations. Because of the fix number of water molecules considered in a given simulation, the relation with *D*-spacing is not straightforward.

The goal of this section is to get insights into SMT interaction with lipid bilayers. In this direction, for experimental studies, EPC liposomes where used as a model of lipid bilayer. First, cryo-TEM was used to analyze EPC liposomes, plain (control) or loaded with different concentrations of SMT. We observed a wide range of liposome sizes (e.g., 0.03–0.5 μm) and structures (e.g., multilamellar, multivesicular, unilamellar, and different combinations). A rough estimation of δm (~ 40 Å) and *D*-spacing of (~ 90 Å) was made by image analysis. When comparing plain (Fig. 2a) with the SMT loaded (Fig. 2b, c, d) EPC liposomes, we observed that the latter shows more circular shapes. Furthermore, liposomes with 11:1 SMT:EPC concentration were found to be mainly unilamellar and smaller than the others (Fig. 2d). In the inset of Fig. 2d, we present a snapshot of a typical multilamellar vesicle found in all studied systems.
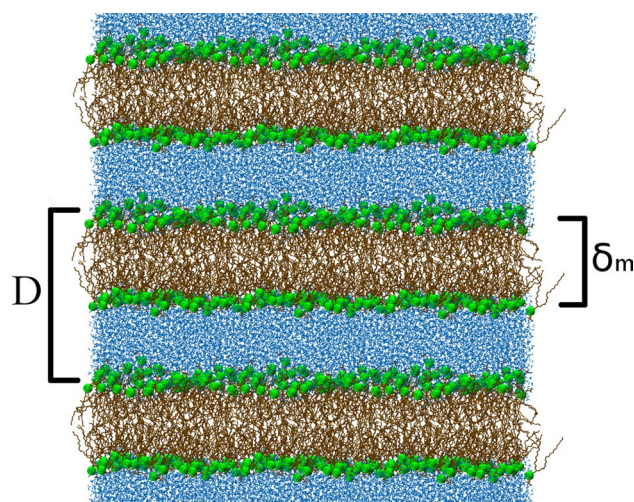

Fig. 1 Schematic representation of multilamellar bilayers. Lipid heads are in green, lipid tails are in brown, and water is in light blue. *D* represented the *D*-spacing and δm the bilayer thickness

Fig. 2 Cryo-TEM images of **a** plain EPC liposomes and **b** 1:1, **c** 1:3 and **d** 11:1 SMT loaded liposomes (SMT: EPC ratio). The inset in **d** is a typical multilamellar structure, observed in all liposome preparations
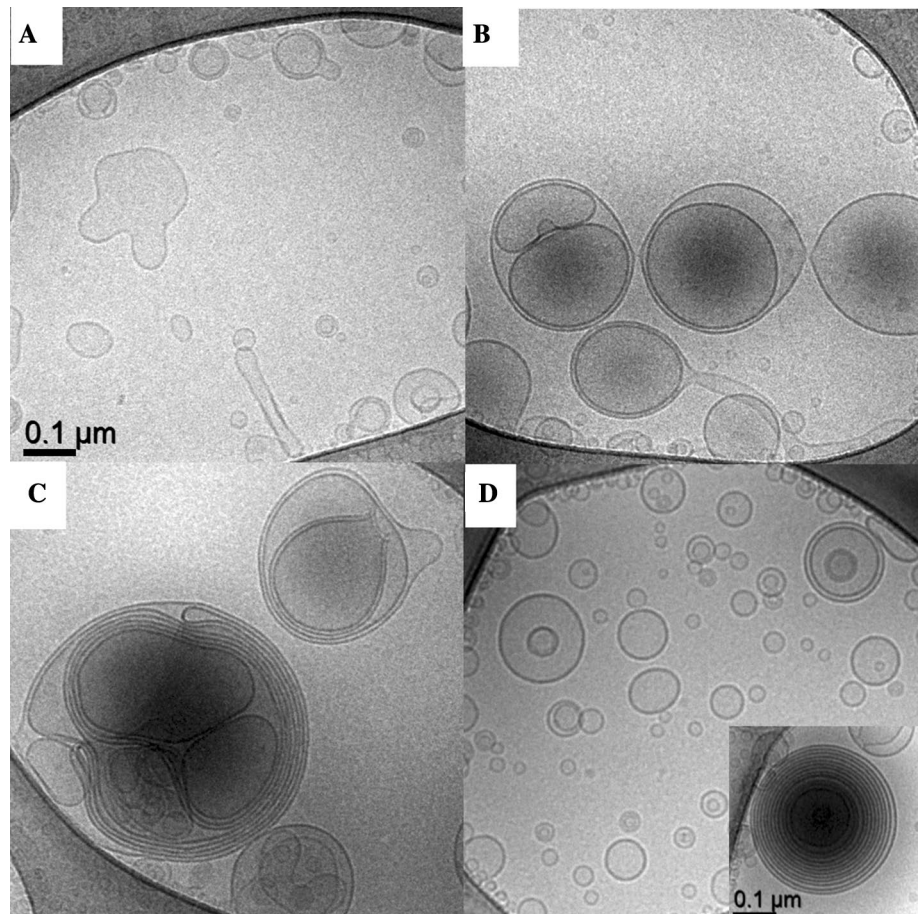

Fig. 3 Experimental SAXS profile for plain liposome (magenta circles), 1:3 (green circles), and 1:2 (orange circles) SMT: lipid molar ratios. The black line corresponds to the fitting of experimental data using the Gaussian deconvolution method mentioned above. **b** Total EDP obtained from SAXS data for plain liposomes (magenta line), 1:3 (green line), and 1:2 (orange line) SMT: lipid ratios
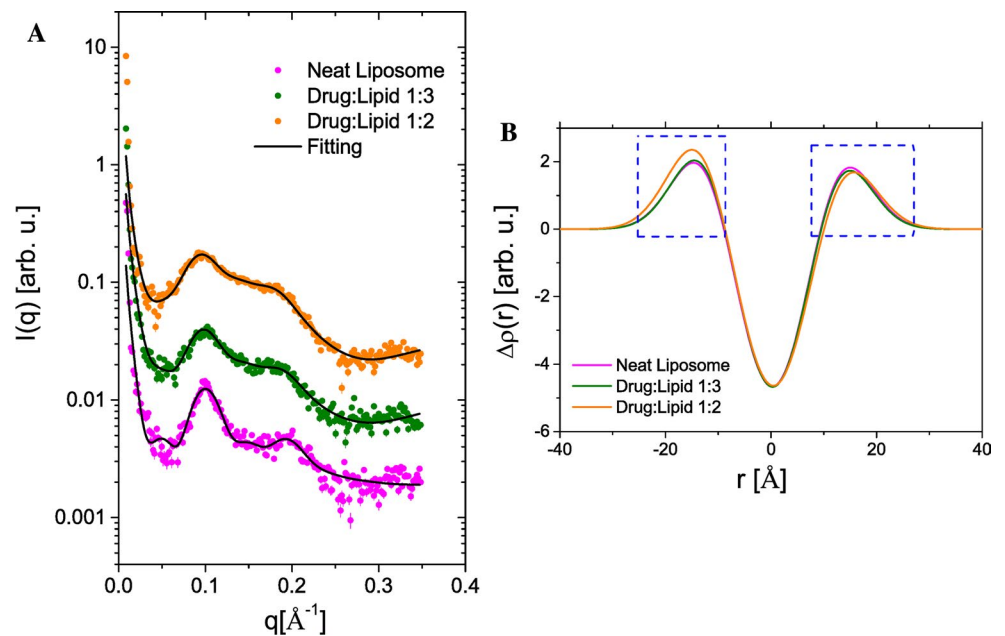
The observed differences in size and shape could be due to the SMT intercalation at the interface, stabilizing the surface tension as a result of its amphiphilic nature and small size.

Then, using SAXS we were able to access more detailed information on the effects of SMT in EPC liposomes. In Fig. 3a, we show the SAXS results for the neat liposomes

and two different molar ratios (1:3 and 1:2 SMT: EPC). The black line corresponds to the fitting of experimental data using the Gaussian deconvolution method (Oliveira et al. 2012). Experimental data are shown as intensity $I(q)$ versus the momentum transfer $q = (4/\lambda) \sin \theta$, where λ is the radiation wavelength and 2θ is the scattering angle. After treatment, the data were normalized to an absolute scale using water as the primary standard as shown in Fig. 3b. The comparison between different concentrations showed differences in the region corresponding to the phosphate peak, indicating that the drug is absorbed in the lipid–water interface. In this direction, SAXS measurements confirmed the interfacial partition of the drug, predicted by MD simulations (Wood and Pickholz 2013). In Table 1, we present the D-spacing, δm, and the number of lamellae (N) for each of the systems, based on the fitting of the modified Caillé theory (Oliveira et al. 2012). The D-spacing increases with the SMT concentrations, going from 62.1 ± 0.4 to 65.8 ± 0.4 Å. However, no significant differences were observed for δm. In this way, the increased hydration of the lipid bilayer in the presence of SMT could be responsible for the differences in the D-spacing.

Both SAXS and cryo-TEM gave us evidence of the interaction of SMT with EPC liposomes. Cryo-Tem pointed out that the shape of the liposomes and the number of lamellae depend on the SMT concentration. In this direction, SAXS supports this behavior, showing a decreasing number of lamellae while increasing SMT concentrations.

**Table 1** Values of adjusted parameters from SAXS experiments

SMT: EPC	D (Å)	N	δm (Å)
Plain	62.1 ± 0.4	2.8 ± 0.2	43 ± 5
1:3	63.4 ± 0.5	2.5 ± 0.1	41 ± 2
1:2	65.8 ± 0.4	2.3 ± 0.1	42 ± 9

Moreover, the δm values quantitatively agree between both techniques (~ 4Å). Comparing SAXS, a more precise quantitative method, with Cryo-TEM, we observed a difference in D-spacing values, probably due to the vesicle selection bias and low-temperature conditions in this last technique.

In light of the SAXS results, we revisited MD simulations corroborating the molecular interfacial behavior (Wood and Pickholz 2013). In the referred work, we reported a molecular dynamics simulations study of SMT in a fully hydrated bilayer of POPC at the fluid lamellar phase. These previous simulations were carried out at three different drug/lipid stoichiometries, 1:75, 1:10, and 1:3, under NPT conditions. Our results showed the partition of SMT between the lipid head group–water interface and water phase. The main interactions that stabilized the drugs in this region were hydrogen bonds, salt bridges, and cation-π. Nevertheless, the samplings using AA simulations are restricted in both time and size.

In order to investigate more complex systems involving SMT by MD simulations at a coarse-grained level, such as SMT drug-delivery systems, an SMT CG model is needed. In this direction, we here developed a SMT CG model based on AA simulations. We chose to build up our model within the widely used MARTINI force field scheme, and in order to do so, we have mapped the 42 atoms in seven beads accounting for the molecular shape and chemical nature, as shown in Fig. 4 (Marrink et al. 2007; Monticelli et al. 2008). Our model represents the protonated form of SMT that prevails at physiological pH (Wojnar-Horton et al. 1996; Wood and Pickholz 2013). To assign the particle type to each bead, we first looked to the chemical functional groups in MARTINI biomolecular structures (Marrink et al. 2007). The indole ring skeleton was taken from that of tryptophan amino acid due to their similarity (Monticelli et al. 2008). For lateral sulfonamide and lateral amino substituents, we made a thoughtful particle selection, among the MFF

Fig. 4 Sumatriptan all-atom (AA) to coarse-grain (CG) mapping scheme. The indole ring skeleton (S2, S4, S5) was taken from that of the tryptophan amino acid in the MFF (sC4). For lateral sulfonamide (S6, 67) and lateral amino substituents (S1, S3), we made a thoughtful particle selection among the MFF particles for different molecular substructures (P5, P3–Qd)
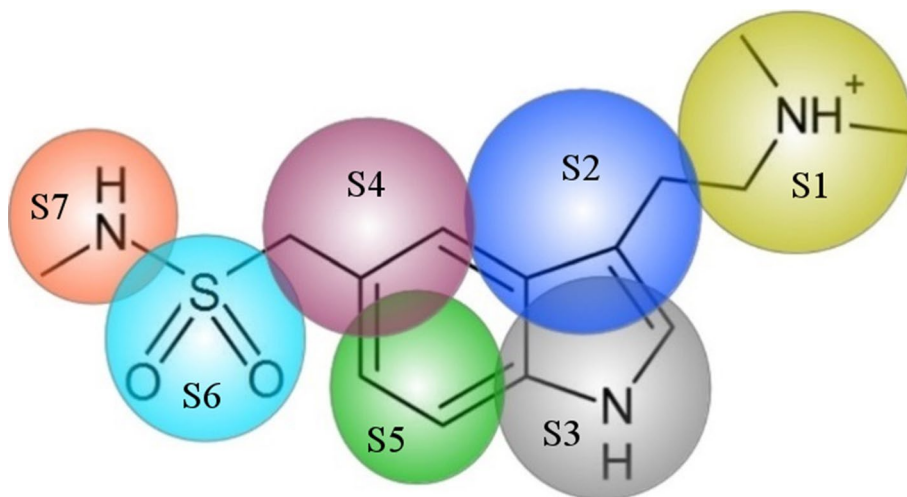
particles for different molecular substructures (Marrink et al. 2007). Van der Waals interactions were based on the chosen CG particle types, while bond lengths, angles, and dihedrals were obtained from geometry optimization of the molecule using quantum chemical calculations (Wood and Pickholz 2013). We performed a fine-tuning of the CG SMT parameter aiming to reproduce the atomistic behavior (Wood and Pickholz 2013). For this purpose, we carried out several simulations of a small POPC lipid bilayer (150 lipids) at 3 SMT:lipid concentrations. The chosen concentrations were 1:75, 1:10, and 1:3 SMT:lipid ratio, following the reference of Wood and Pickholz (2013). We chose the parameters that were able to reproduce semi-quantitatively the atomistic percentages of molecules in different regions, at the three different drug concentrations (Wood and Pickholz 2013). These parameters could be found in additional material section (Supplementary Material).

We found good agreement between the AA and CG simulations results. The partition of the molecules in the different regions is a dynamical process also captured by the CG model. In order to illustrate this, in Fig. 5 we show the electron density profile (EDP) for the AA and CG simulations for the three studied concentrations. $z = 0$ corresponds to the bilayer center. As have we already discussed, SMT partitioned between the water and lipid–water interface in all cases. We quantified the amount of SMT for AA and CG simulation at the three concentrations in different regions.
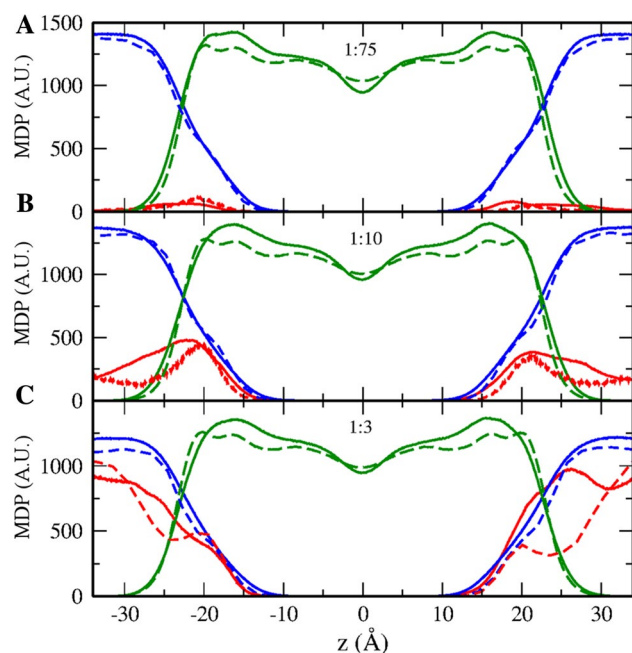

Fig. 5 Overlap of the electron density profiles of all atom (dashed lines) and coarse-grained simulations (solid lines) at three different SMT:lipid molar ratios: 1:75 (**a**), 1:10 (**b**), and 1:3 (**c**). The POPC electron density profile is depicted in green, water is in blue, and SMT is in red

Because the integration was done over the EDP, it was averaged the SMT is a dynamical process in each region both in AA as well as CG simulations. The bilayer was divided into three main regions: a bulk aqueous phase (ranging from the z-box edge until ± 27 Å), a bilayer–water interface (co-existence of polar heads and associated waters ranging from ± 27 to ± 15 Å), and a hydrophobic region of the bilayer, where water density is very low (in the range of ± 15 Å). Results are summarized in Table 2 were the good agreement between the AA and CG models can be observed. We then had a suitable SMT CG model to study different systems involving SMT. In this direction, in the following section, we present the results obtained when testing it in a PL micelle.

Sumatriptan in Pluronic F127 polymeric micelles

We have chosen PL F127 micelles as a model to test the CG SMT in a drug-delivery system. PL F127 micelles are well-defined physicochemical systems that could be accessible by MD simulations as we have already explored in previous work (Wood et al. 2016). In this section, we first simulated the micelles with and without SMT at a coarse-grained level followed by experimental validation of these micellar systems.

In our simulations, 100 PL F127 molecules were arranged to have the hydrophobic PPO beads inside the core surrounded by the PEO ones, resulting in a pre-assemble plain micelle. The micelle was solvated in polarizable water beads (Yesylevskyy et al. 2010), as explained in the Materials and methods section. The plain micelle was equilibrated and ran up to 1 µs. The micelle overall organization was studied by centering it at PPO center of mass. We calculated its radial density profile (*rDP*), averaged over the last 500 ns of the simulation run, as a function of the radius r (see Fig. 6a) (Pickholz and Giupponi 2010). In Fig. 5b, we show the rDP of the different system components: total poloxamer (black), separated in hydrophilic (PEO) (green), and hydrophobic blocks (PPO) (red), and water (blue). PPO distribution is localized and does not have contact with the aqueous face. Around PPO, PEO blocks have shown an extended distribution, with little access to the hydrophobic region. Also, PEO blocks form a PEO water interface. Besides, we observed the presence of a small amount of water and PEO inside the micellar core.

Table 2 Number of SMT molecules from AA and CG simulations at different concentrations

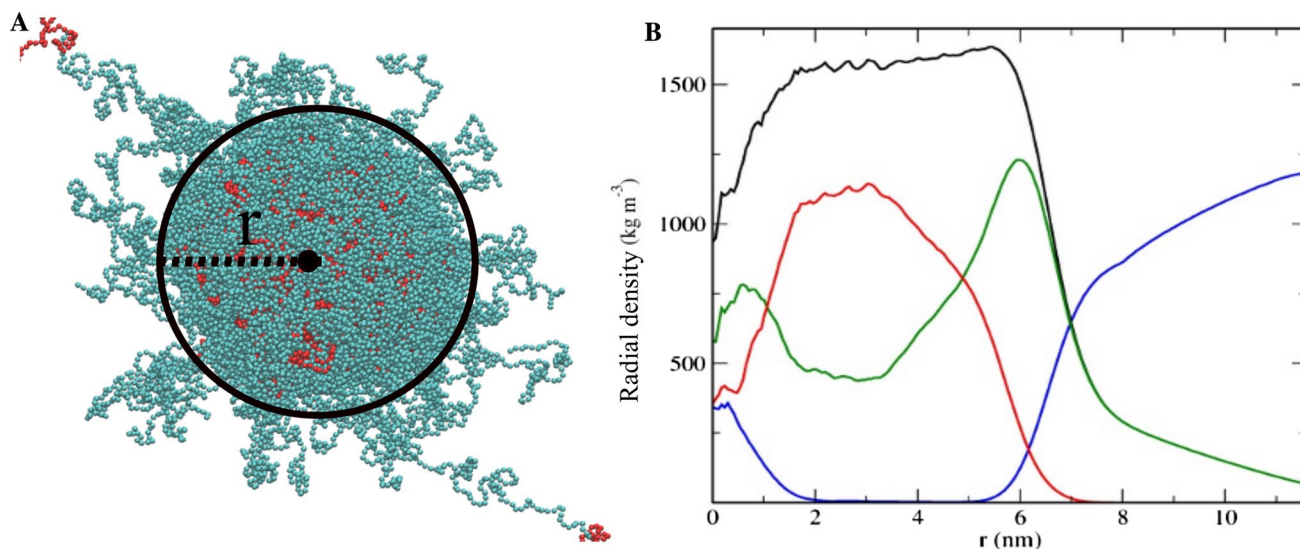| SMT:Lipid	1:75	1:10	1:3
Level	*AA*:*CG*	*AA*:*CG*	*AA*:*CG*
Water	21:23	32:46	64:65
Interface	77:76	66:53	36:35
Membrane	2:1	2:1	0:0

Fig. 6 **a** Preassembled F127 micelle representation: PPO beads are in red, PEO beads are in green, and water is in blue. Radius r is also shown, $r = 0$ Å, which corresponds to the center of mass of the PPO core. **b** Radial density profile of F127 preassembled system over ~ 500 ns. The F127 density is depicted in black, the PPO in red, the PEO in green, and water in blue

Fig. 7 **a** *SMT-in* and **b** *SMT-out* systems representative snapshots: molecules are represented in purple, PEO in green, and PPO in red. Water molecules are not explicitly shown for better visualization. **c** *SMT-in* and **b** *SMT-out* systems. Radial density profile: SMT in purple, F127 density is depicted in black, PPO in red, PEO in green, and water in blue
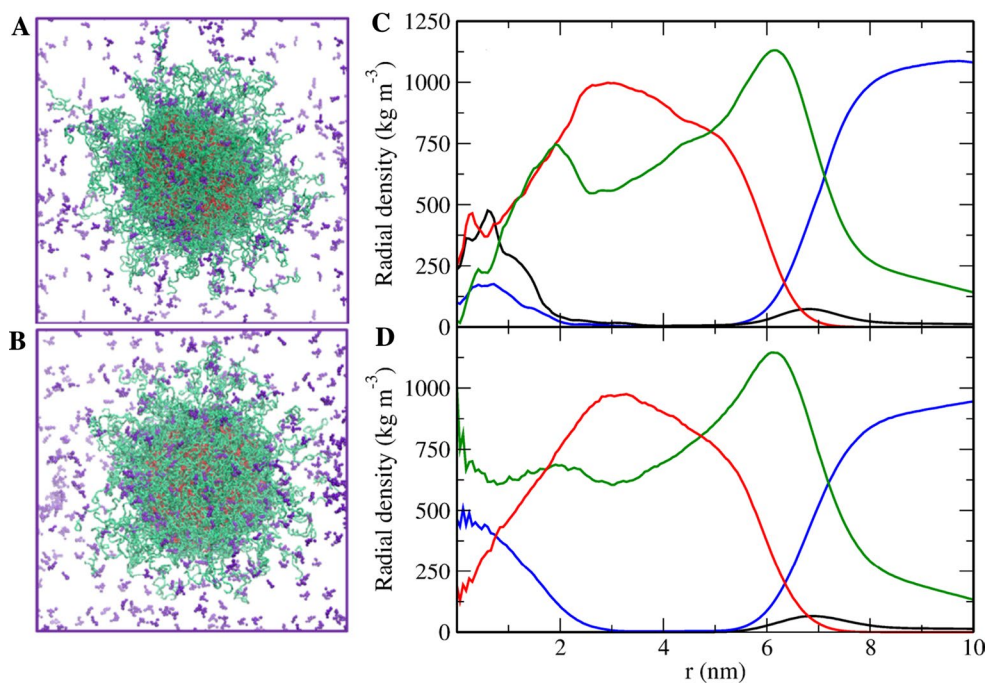
Our next step was to investigate the SMT interaction with these preassembled systems. In this regard, we have added SMT molecules from two different initial conditions: placing the drug in the external phase (*SMT-out*) and inside, in the PPO core (*SMT-in*). In both cases, the SMT:F127 molar ratio was 3:1. We ran both systems, up to 1 μs. In Fig. 7a and b, we show a snapshot of each simulated system. At first glance, both systems seem similar: SMT molecules partitioned between the aqueous phase and the micelle structure.

In order to make a quantitative analysis of the components distribution, in Fig. 7c and d we show the radial distribution function (rDP) for the different components of both systems. The PPO distribution was essentially observed at micelle core, and PEO distribution extends along the whole system, with higher density at the water–micelle interphase, as described for F127 plain micelles (Wood et al. 2016). Also, a few water molecules were found on the micelle core, as previously described for similar systems, without

the drug. SMT essentially partition between the hydrophilic core–water interface and the water phase. Besides, for the *SMT-in* case, few molecules are trapped in the micelle core, where a little hydrophilic environment is found (presence of PEO and water, as discussed). The SMT distribution, at the hydrophilic crown, matches for both cases. This behavior is in line with the interfacial distribution observed for protonated SMT in lipid bilayers discussed here in "Sumatriptan interaction with lipid bilayers: building up the coarse-grained model" section.

To determine the dynamics of the encapsulation of SMT within the micelles, we calculated the number of SMT molecules "inside" as a function of time. Because of the interface extension, the radius defining the boundaries of the micelle is not strictly well defined. In this way, we have considered three different radii ($r = 8$, 8.5, and 9 nm) in order to account for this range/variation/fluctuation. In Fig. 8, we show the number of SMT inside for both initial conditions and the three r values. Considering shorter radius, we were able to quantify two molecules trapped in the micellar core for the *SMT-in* case. Furthermore, the average number of SMT at the interface matched between both *in* and *out* cases ($\sim 276 \pm 6$ molecules). The encapsulation time evolution accounts on the SMT attaching and detaching dynamical behavior (Fig. 8), also observed by trajectory analysis (results not shown).

To contrast our simulation with experimental data, PL F127 micelles with and without SMT were also studied using experimental techniques, as explained in the Materials and methods section. The plain and SMT-loaded micelles

(1:1 molar concentration of SMT: F127) were characterized by DLS and z-potential measurements. Given the thermo-sensitive behavior reported for these systems, we choose to work at two temperatures, $T = 37$ and 45 °C (Basak and Bandyopadhyay 2013). Because of the similarity of the results obtained at both temperatures, in most of the discussion we will refer to 37 °C.

Size information about these systems was obtained by DLS measurements. In these experiments, the normalized temporal autocorrelation functions of the experimental intensity fluctuations (raw correlation) were obtained. This function, together with an exponential fitting, is shown in Fig. 9a for both cases (Meller et al. 1998). Besides, these raw correlation data were analyzed to extract information on size distribution (Bhattacharjee 2016). The diffusion coefficients were obtained by fitting the raw correlation function with a suitable algorithm. Two methods of analysis are used: cumulants and distribution analysis. Through cumulants analysis, we determined the mean size and polydispersity index (PDI, shown in Fig. 9b (Maulucci et al. 2005). On the other hand, distribution analysis determined the actual size distribution with the CONTIN algorithm (Varga et al. 2014) (see Fig. 8c). Mie theory (Ross and Sigel 2012) can be applied to represent the size distribution in volume. From it, the number size distribution can then be calculated from simple geometrical considerations. The distribution analysis transformation from intensity to volume or number makes the following assumptions: all particles are spherical; all particles have a homogeneous equivalent density, and the optical properties are known (Bhattacharjee 2016). A similar

Fig. 8 Time evolution of the number of SMT molecules inside the micelle (red and black curves correspond to -in and -out initial conditions, respectively). We consider three different radii: **a** $r = 8.0$ nm, **b** $r = 8.5$ nm, and **c** $r = 9.0$ nm
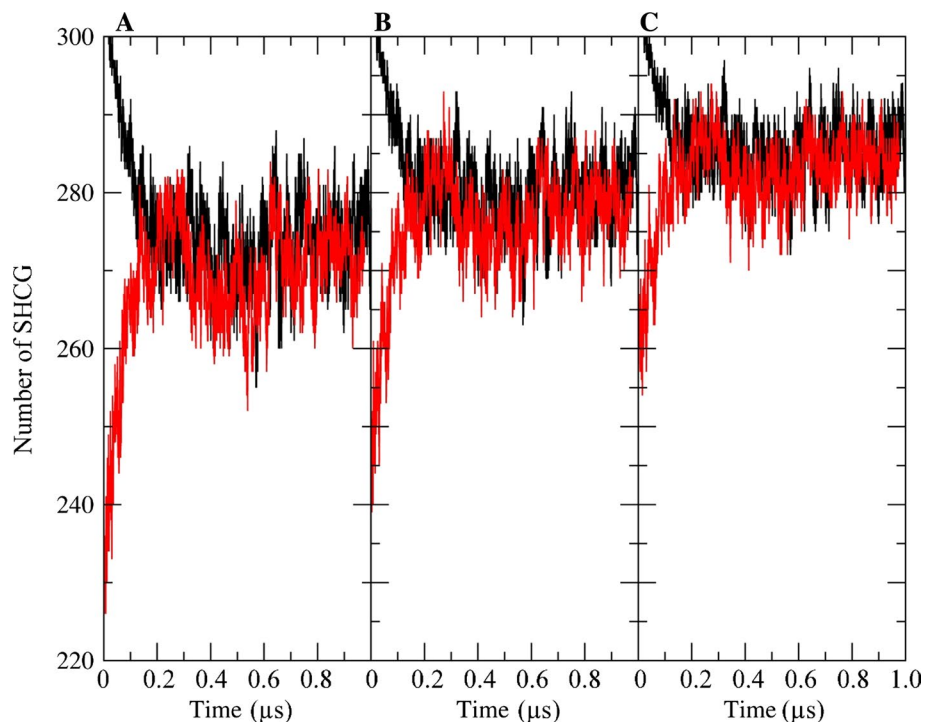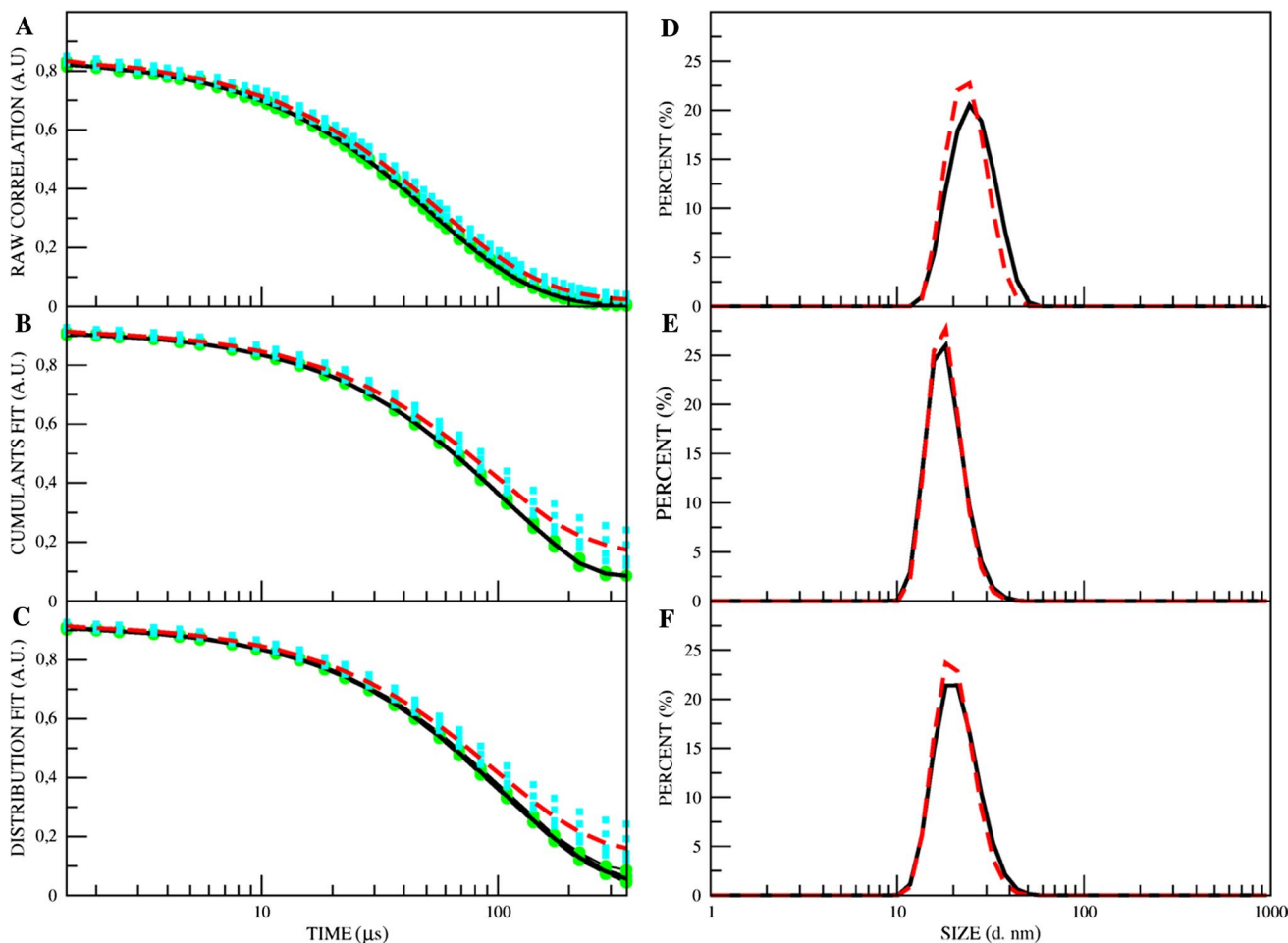
Fig. 9 DLS measurements. Raw correlation data (**a**), cumulants fit (**b**), and distribution fit (**c**) data from DLS analysis. In cyan and green the data from SMT and plain micelles are plot with a fit in red-dashed and black-full representations. Intensity (**d**), number (**e**), and volume (**f**) percentage of populations against the hydrodynamic size where the black line is the plain micelles and the red dashed line is the SMT-loaded ones

size distribution between intensity, number, and volume (all of them analyzed here) is expected for a homogeneous colloidal system. In Fig. 9, we show the intensity (Fig. 9d), number (Fig. 9e), and volume (Fig. 9f) percentage of the populations as a function of the diameter size. Combining the three-distribution analysis, we can characterize a homogeneous population of 25 nm of hydrodynamic diameter. Moreover, the differences between the plain (black) and loaded (red) micelles are subtle, indicating that the presence

of SMT in the polymeric micelles does not affect the average size. In Table 3, we summarized the main results including the $T = 45\,°C$. We would like to remark that the results are very similar at both temperatures; the main differences were observed for PDI, which decrease from 0.211 to 0.193 when increasing the temperature. These results were also in good agreement with DLS measurements done by Oshiro et al. (2014) for sumatriptan-loaded micelles at 37 °C. With our simulations, we were able to reach experimentally relevant

Table 3 Comparison of micelles, with and without SMT, at different temperatures

Temp (°C)	37			45		
SMT:PL	Size (nm)	PDI	Z-potential (mV)	Size (nm)	PDI	Z-potential (mV)
0:1	24.22 ± 0.471	0.063 ± 0.030	− 1.71 ± 1.75	24 ± 0.1372	0.049 ± 0.015	− 2.1 ± 1.87
1:1	25.22 ± 0.248	0.211 ± 0.024	2.96 ± 0.672	25 ± 0.3635	0.193 ± 0.031	2.96 ± 0.96

Z-potential changes were observed between the two formulations regardless of the temperature

micelle size. The simulated micelles are approximately 17 nm, according to the experimental range. It is important to take into account the over-estimation of the hydrodynamic diameter and the PDI. Besides, both experimental and simulation approaches showed no changes on micelle size in the presence of SMT. Evidence of SMT encapsulation needs to be obtained by other methods.

The electron kinetic surface potential, also known as the Zeta-potential, yields information on the surface charge distribution of colloidal systems (Ito et al. 2004). In this direction, we measured this property in order to evaluate the SMT effects on the poloxamer micelle surface. In Table 2, we show the results for the studied systems, where no differences were found between the two studied temperatures. The main results observed with this technique were that the presence of the drug had a significant impact on Z-potential, shifting it from − 1.71 mV (plain) to 2.96 mV (SMT-loaded). This is strong evidence of SMT affecting the micelle surface charge distribution. The simulations carried out in this work could give an explanation of these phenomena, considering the described SMT partition in PEO–water interface that would alter the surface charge.

The simulated micelles reproduced both micelle size and interfacial distribution of the drug in good agreement with DLS and Z-potential analysis. In this sense, micelles systems were a good environment under which we were able to test our newly developed SMT CG model.

Conclusions

In this work, we successfully developed and tested a CG model for sumatriptan. This development was based on results from atomistic simulation (Wood and Pickholz 2013, 2014), corroborated by experimental techniques shown here. The SMT CG model presented here expands the possibilities to explore the encapsulation of sumatriptan in different drug-delivery systems. In this sense, we would like to highlight the power of computer simulations at the coarse-grained level, when combined with experiments, as a tool to shed light on biological and nanotechnological systems.

References

Basak R, Bandyopadhyay R (2013) Encapsulation of hydrophobic drugs in Pluronic F127 micelles: effects of drug hydrophobicity, solution temperature, and pH. Langmuir 29:4350–4356. https://doi.org/10.1021/la304836e

Berendsen HJC, Postma JPM, van Gunsteren WF et al (1984) Molecular dynamics with coupling to an external bath. J Chem Phys 81:3684–3690. https://doi.org/10.1063/1.448118

Bhattacharjee S (2016) DLS and zeta potential—What they are and what they are not?. Elsevier, Amsterdam

Cereda CMS, Brunetto GB, de Araújo DR, de Paula E (2006) Liposomal formulations of prilocaine, lidocaine and mepivacaine prolong analgesic duration. Can J Anesth 53:1092–1097. https://doi.org/10.1007/BF03022876

Gasperini AAM, Puentes-Martinez XE, Balbino TA et al (2015) Association between cationic liposomes and low molecular weight hyaluronic acid. Langmuir 31:3308–3317. https://doi.org/10.1021/la5045865

Girotra P, Singh SK (2016) A comparative study of orally delivered PBCA and ApoE coupled BSA nanoparticles for brain targeting of sumatriptan succinate in therapeutic management of migraine. Pharm Res 33:1682–1695. https://doi.org/10.1007/s11095-016-1910-8

Gulati N (2013) Intranasal delivery of chitosan nanoparticles for migraine therapy. Sci Pharm 81:843–854. https://doi.org/10.3797/scipharm.1208-18

Haddish-Berhane N, Rickus JL, Haghighi K (2007) The role of multiscale computational approaches for rational design of conventional and nanoparticle oral drug delivery systems. Int J Nanomedicine 2:315–331

Hansraj GP, Singh SK, Kumar P (2015) Sumatriptan succinate loaded chitosan solid lipid nanoparticles for enhanced anti-migraine potential. Int J Biol Macromol 81:467–476. https://doi.org/10.1016/j.ijbiomac.2015.08.035

Hassan PA, Rana S, Verma G (2015) Making sense of Brownian motion: colloid characterization by dynamic light scattering. Langmuir 31:3–12. https://doi.org/10.1021/la501789z

Hess B, Kutzner C, van der Spoel D, Lindahl E (2008) GROMACS 4: algorithms for highly efficient, load balanced, and scalable molecular simulations. J Chem Theory Comput 4:435–447

Horn JN, Kao T-C , Grossfield A (2014) Coarse-grained molecular dynamics provides insight into the interactions of lipids and cholesterol with rhodopsin. In: Advances in experimental medicine and biology. Springer, Netherlands. https://doi.org/10.1007/978-94-007-7423-0_5

Ito T, Sun L, Bevan MA, Crooks RM (2004) Comparison of nanoparticle size and electrophoretic mobility measurements using a carbon-nanotube-based coulter counter, dynamic light scattering, transmission electron microscopy, and phase analysis light scattering. Langmuir 20:6940–6945. https://doi.org/10.1021/la049524t

Karplus M, McCammon JA (2002) Molecular dynamics simulations of biomolecules. Nat Struct Biol 9:646–652. https://doi.org/10.1038/nsb0902-646

Marrink SJ, Risselada HJ, Yefimov S et al (2007) The MARTINI force field: coarse-grained model for biomolecular simulations. J Phys Chem B 111:7812–7824. https://doi.org/10.1021/jp071097f

Maulucci G, De Spirito M, Arcovito G et al (2005) Particle size distribution in DMPC vesicles solutions undergoing different sonication times. https://doi.org/10.1529/biophysj.104.048876

Meller A, Bar-Ziv R, Tlusty T et al (1998) Localized dynamic light scattering: a new approach to dynamic measurements in optical microscopy. Biophys J 74:1541–1548. https://doi.org/10.1016/s0006-3495(98)77866-x

Monticelli L, Kandasamy SK, Periole X et al (2008) The MARTINI coarse-grained force field: extension to proteins. J Chem Theory Comput 4:819–834. https://doi.org/10.1021/ct700324x

Oliveira CLP, Gerbelli BB, Silva ERT et al (2012) Gaussian deconvolution: a useful method for a form-free modeling of scattering data from mono- and multilayered planar systems. J Appl Crystallogr 45:1278–1286. https://doi.org/10.1107/S002188981204191X

Oshiro A, Silva DC, De Mello JC et al (2014) Pluronics F—127/L-81 binary hydrogels as drug-delivery systems: influence of physicochemical aspects on release kinetics and cytotoxicity. Langmuir 30:13689–13698

Patil YP, Jadhav S (2014) Novel methods for liposome preparation. Chem Phys Lipids 177:8–18

Pedersen JS, Oliveira CLP, Hübschmann HB et al (2012) Structure of immune stimulating complex matrices and immune stimulating complexes in suspension determined by small-angle X-ray scattering. Biophys J 102:2372–2380. https://doi.org/10.1016/j.bpj.2012.03.071

Pickholz M, Giupponi G (2010) Coarse-grained simulations of local anesthetics encapsulated into a liposome. J Phys Chem B 114:7009–7015. https://doi.org/10.1021/jp909148n

Ross DJ, Sigel R (2012) Mie scattering by soft core-shell particles and its applications to ellipsometric light scattering. Phys Rev E 85:56710. https://doi.org/10.1103/PhysRevE.85.056710

Sharma PK, Bhatia SR (2004) Effect of anti-inflammatories on Pluronic® F127: micellar assembly, gelation and partitioning. Int J Pharm 278:361–377. https://doi.org/10.1016/j.ijpharm.2004.03.029

Steichen SD, Caldorera-Moore M, Peppas NA (2013) A review of current nanoparticle and targeting moieties for the delivery of cancer therapeutics. Eur J Pharm Sci 48:416–427

Tepper SJ, Rapoport AM, Sheftell FD (2002) Mechanisms of action of the 5-HT1B/1D receptor agonists. Arch Neurol 59:1084–1088

Tfelt-Hansen PC (2010) Does sumatriptan cross the blood–brain barrier in animals and man? J Headache Pain 11:5–12. https://doi.org/10.1007/s10194-009-0170-y

Varga Z, Yuana Y, Grootemaat AE et al (2014) Towards traceable size determination of extracellular vesicles. J Extracell Vesicles. https://doi.org/10.3402/jev.v3.23298

Wojnar-Horton RE, Hackett LP, Yapp P et al (1996) Distribution and excretion of sumatriptan in human milk. Br J Clin Pharmacol 41:217–221. https://doi.org/10.1111/j.1365-2125.1996.tb00185.x

Wood I, Pickholz M (2013) Concentration effects of sumatriptan on the properties of model membranes by molecular dynamics simulations. Eur Biophys J 42:833–841. https://doi.org/10.1007/s00249-013-0932-y

Wood I, Pickholz M (2014) Triptan partition in model membranes. J Mol Model 20:1–8. https://doi.org/10.1007/s00894-014-2463-6

Wood I, Martini MF, Albano JMR et al (2016) Coarse-grained study of pluronic F127: Comparison with shorter co-polymers in its interaction with lipid bilayers and self-aggregation in water. J Mol Struct 1109:106–113. https://doi.org/10.1016/j.molstruc.2015.12.073

Yesylevskyy SO, Schäfer LV, Sengupta D, Marrink SJ (2010) Polarizable water model for the coarse-grained MARTINI force field. PLoS Comput Biol 6:1–17. https://doi.org/10.1371/journal.pcbi.1000810

Zhang Y, Lam YM (2007) Controlled synthesis and association behavior of graft Pluronic in aqueous solutions. J Colloid Interface Sci 306:398–404. https://doi.org/10.1016/j.jcis.2006.10.073